

# New tracker models of dark energy

Satadru Bag,<sup>a</sup> Swagat S. Mishra<sup>a</sup> and Varun Sahni<sup>a</sup>

<sup>a</sup>Inter-University Centre for Astronomy and Astrophysics, Post Bag 4, Ganeshkhind, Pune 411 007, India

E-mail: [satadru@iucaa.in](mailto:satadru@iucaa.in), [swagat@iucaa.in](mailto:swagat@iucaa.in), [varun@iucaa.in](mailto:varun@iucaa.in)

**Abstract.** We describe a new class of dark energy (DE) models which behave like cosmological trackers at early times. These models are based on the  $\alpha$ -attractor set of potentials, originally discussed in the context of inflation. The new models allow the current acceleration of the universe to be reached from a wide class of initial conditions. Prominent examples of this class of models are the potentials  $\coth\varphi$  and  $\cosh\varphi$ . A remarkable feature of this new class of models is that they lead to large enough negative values of the equation of state at the present epoch, consistent with the observations of accelerated expansion of the universe, from a very large initial basin of attraction. They therefore avoid the fine tuning problem which afflicts many models of DE.

**Keywords:** Dark energy, tracker potential,  $\alpha$ -attractor

---

## Contents

<b>1</b>	<b>Introduction</b>	<b>1</b>
<b>2</b>	<b>Conformal inflation and <math>\alpha</math>-attractors</b>	<b>2</b>
<b>3</b>	<b>Tracker Models of Dark Energy</b>	<b>5</b>
3.1	L-model	5
3.2	Oscillatory tracker model	8
3.3	The Recliner model	13
3.4	Transient dark energy from the Margarita potential	14
<b>4</b>	<b>Discussion</b>	<b>20</b>
<b>A</b>	<b>Can <math>\Lambda</math>CDM cosmology emerge from a single oscillatory potential ?</b>	<b>21</b>

---

## 1 Introduction

A remarkable property of our universe is that it appears to be accelerating. Within the context of Einstein’s theory of general relativity, cosmic acceleration can arise if at least one of the constituents of the universe violates the strong energy condition  $\rho + 3p \geq 0$ . Physical models with this property are frequently referred to as ‘dark energy’ (DE). Although several models of DE have been advanced in the literature, perhaps the simplest remains Einstein’s original idea of the cosmological constant,  $\Lambda$ . As its name suggests, the energy density associated with the cosmological constant,  $\frac{\Lambda}{8\pi G}$ , and its equation of state,  $w = -1$ , remain the same at all cosmological epochs. Although  $w = -1$  satisfies current observations very well, the non-evolving nature of  $\Lambda$  implies an enormous difference in its density and that in matter or radiation at early times. For instance  $\rho_\Lambda/\rho_r \sim 10^{-58}$  at the time of the electroweak phase transition, at earlier times this ratio is still smaller.

This ‘imbalance’ between the non-evolving and small value of  $\Lambda$  on the one hand, and the evolving density in matter/radiation on the other, has fueled interest in models in which, like matter/radiation, DE also evolves with time [1–3]. In this context, considerable attention has been focused on models with ‘tracker’ properties which enable the present value of the DE density to be reached from a wide range of initial conditions. This class of models appears to alleviate the so-called ‘fine-tuning’ (or ‘initial value’) problem which characterizes  $\Lambda$  [4–12]. A scalar field with the inverse power-law (IPL) potential  $V \propto \varphi^{-\alpha}$  ( $\alpha > 0$ ), presents one of the oldest and best studied examples of this class of models [4, 5]. Unfortunately the IPL model cannot account for the large negative values of  $w_{\text{DE}}$  at the present epoch consistent with the observations [13–17] while at the same time preserving a large initial basin of attraction [7, 8].

In this paper we describe a new class of DE models based on the  $\alpha$ -attractors [18, 19]. A compelling feature of these new models is that they have a very wide basin of attraction which allows the late time asymptote  $w = -1$  to be reached from a large class of initial conditions. A total of four different DE models are described in this paper. Each of these models has very distinctive features which are reflected in the evolution of  $w_\varphi(z)$  and its first derivative,  $w' = dw_\varphi/d\ln a$ . An interesting property of these models is that their current equation of state (EOS) can drop below  $-0.9$ , providing good agreement with present observational bounds. Our results lead us to conclude that tracker models of DE could be very relevant for the understanding of cosmic acceleration.

The plan of our paper is as follows: The  $\alpha$ -attractor family of potentials is briefly discussed in section 2. Section 3 contains our main results and provides an analysis of the four new models of tracker dark energy. A summary of our results is presented in section 4.

## 2 Conformal inflation and $\alpha$ -attractors

Kalosh & Linde recently discovered an interesting new family of potentials which could give rise to successful inflation [18]. They noted that the Lagrangian

$$\mathcal{L} = \sqrt{-g} \left[ \frac{1}{2} \partial_\mu \chi \partial^\mu \chi + \frac{\chi^2}{12} R(g) - \frac{1}{2} \partial_\mu \phi \partial^\mu \phi - \frac{\phi^2}{12} R(g) - \frac{\tilde{\lambda}}{4} (\phi^2 - \chi^2)^2 \right], \quad (2.1)$$

where  $\tilde{\lambda}$  is a dimensionless parameter and  $\chi, \phi$  are scalar fields, is invariant under the  $O(1, 1)$  group of transformations in the  $(\chi, \phi)$  space and also under the group of local conformal transformations. Fixing the local conformal gauge to

$$\chi^2 - \phi^2 = 6m_p^2, \quad (2.2)$$

the Lagrangian in (2.1) can be parameterized by

$$\chi = \sqrt{6}m_p \cosh \frac{\varphi}{\sqrt{6}m_p}, \quad \phi = \sqrt{6}m_p \sinh \frac{\varphi}{\sqrt{6}m_p}, \quad (2.3)$$

so that

$$\frac{\phi}{\chi} = \tanh \frac{\varphi}{\sqrt{6}m_p}. \quad (2.4)$$

Consequently (2.1) reduces to

$$\mathcal{L} = \sqrt{-g} \left[ \frac{m_p^2}{2} R - \frac{1}{2} \partial_\mu \varphi \partial^\mu \varphi - \Lambda m_p^2 \right], \quad (2.5)$$

which describes general relativity with the cosmological constant  $\Lambda = 9\tilde{\lambda}m_p^2$  (here  $m_p = 1/\sqrt{8\pi G} \approx 2.4 \times 10^{18}$  GeV). A conformally invariant generalization of (2.1)

and (2.5),  $\Lambda \rightarrow F(\phi/\chi)m_p^2$ , with an arbitrary function  $F$  that deforms the  $O(1,1)$  symmetry, results in the Lagrangian

$$\mathcal{L} = \sqrt{-g} \left[ \frac{m_p^2}{2} R - \frac{1}{2} \partial_\mu \varphi \partial^\mu \varphi - V(\varphi) \right] \quad (2.6)$$

with the scalar-field potential

$$V(\varphi) = m_p^4 F \left( \tanh \frac{\varphi}{\sqrt{6}m_p} \right). \quad (2.7)$$

Different canonical potentials  $V(\varphi)$  were discussed in [18] in the context of inflation, while [19] introduced the  $\alpha$ -attractor family of potentials following the prescription<sup>1</sup>  $V(\varphi) \rightarrow V(\varphi/\sqrt{\alpha})$ . An attractive feature of the  $\alpha$ -attractors is that they are able to parameterize a wide variety of inflationary scenarios within a common setting.

In [20] it was shown that, in addition to defining inflationary models, the  $\alpha$ -attractors were also able to source oscillatory models of dark matter and dark energy<sup>2</sup>. In this paper we extend the study of [20] by showing that the  $\alpha$ -attractors can give rise to new models of tracker-DE in which the equation of state (EOS) approaches the late-time value  $w \simeq -1$  from a wide class of initial conditions.

In this paper our focus will be on the  $\alpha$ -attractor family of potentials characterized by

$$V(\varphi) = m_p^4 F \left( \tanh \frac{\varphi}{\sqrt{6\alpha}m_p} \right). \quad (2.8)$$

Accordingly, our dark energy models are based on the following potentials all of which have interesting tracker properties:

1. The L-model

$$V(\varphi) = V_0 \coth \left( \frac{\lambda\varphi}{m_p} \right) \quad (2.9)$$

equivalently  $V(\varphi) = V_0 \left[ \tanh \frac{\lambda\varphi}{m_p} \right]^{-1}$ .

2. The Oscillatory tracker model

$$V(\varphi) = V_0 \cosh \left( \frac{\lambda\varphi}{m_p} \right) \quad (2.10)$$

equivalently  $V(\varphi) = V_0 \left[ 1 - \tanh^2 \left( \frac{\lambda\varphi}{m_p} \right) \right]^{-1/2}$ .

---

<sup>1</sup>The parameter  $\alpha$  can be related to the curvature of the superconformal Kähler metric [19].

<sup>2</sup>DE from  $\alpha$ -attractors has also been discussed in [21], although not in the tracker context.

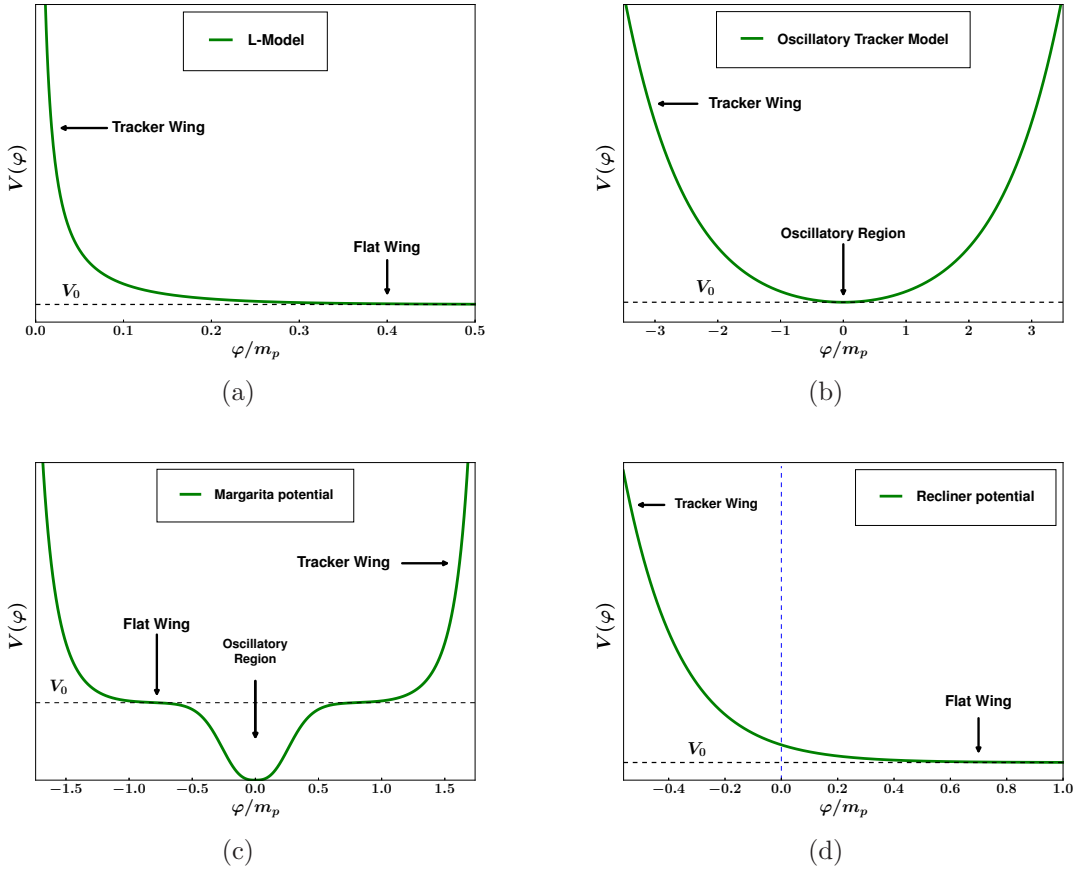


**Figure 1.** Potentials corresponding to different tracker models of dark energy are schematically displayed. Clockwise from the upper left: The L-model (2.9), the Oscillatory tracker model (2.10), the Recliner potential (2.11) and the Margarita potential (2.12).

### 3. The Recliner model

$$V(\varphi) = V_0 \left[ 1 + \exp\left(-\frac{\lambda\varphi}{m_p}\right) \right] \quad (2.11)$$

equivalently  $V(\varphi) = V_0 \left[ 1 + \tanh\left(\frac{\lambda\varphi}{2m_p}\right) \right]^{-1}$ .

### 4. The Margarita potential

$$V(\varphi) = V_0 \tanh^2\left(\frac{\lambda_1\varphi}{m_p}\right) \cosh\left(\frac{\lambda_2\varphi}{m_p}\right) \quad (2.12)$$

where  $\lambda_1 \gg \lambda_2$ .

The tracker parameter  $\lambda$  in our models is related to the parameter  $\alpha$  in (2.8) by

$$\lambda = \sqrt{\frac{1}{6\alpha}}. \quad (2.13)$$

The reader might like to note that in terms of the variable  $x = \tanh \varphi$ , the original  $\alpha$ -attractor based T-model of Inflation [18] is simply  $F(x) = x$  in (2.8), while our L-model is  $F(x) = 1/x$ . The functional form of  $F(x)$  for our remaining three DE models is somewhat more complicated:  $F(x) = (1 - x^2)^{-1/2}$ , for the oscillatory tracker (2.10);  $F(x) = \frac{1}{1+x}$  for the recliner potential (2.11); and finally  $F(x) = \frac{x^2}{\sqrt{1-x^2}}$  for the Margarita potential (2.12). Therefore, from the  $\alpha$ -attractor perspective, the L-model (2.9) appears to be the most appealing of the four DE models introduced by us. One should also point out that, in addition to the above four models, hyperbolic potentials have also been used in connection with the following models of dark energy.

- DE with a constant equation of state  $-1 < w < 0$  is described by [1, 2]

$$V(\varphi) = \frac{3H_0^2(1-w)(1-\Omega_{m0})^{1/|w|}}{16\pi G\Omega_{m0}^\alpha} \left[ \sinh \left( |w| \sqrt{\frac{6\pi G}{1+w}} (\varphi - \varphi_0 + \varphi_1) \right) \right]^{-2\alpha}, \quad (2.14)$$

where

$$\alpha = \frac{1+w}{|w|}, \quad \varphi_0 = \varphi(t_0), \quad \varphi_1 = \sqrt{\frac{1+w}{6\pi G}} \frac{1}{|w|} \ln \frac{1 + \sqrt{1 - \Omega_{m0}}}{\sqrt{\Omega_{m0}}}.$$

- The Chaplygin gas with  $p = -A/\rho$  can be described by the scalar field potential [22, 23]

$$V(\varphi) = \frac{\sqrt{A}}{2} \left( \cosh(2\sqrt{6\pi G}\varphi) + \frac{1}{\cosh(2\sqrt{6\pi G}\varphi)} \right). \quad (2.15)$$

Note that the Chaplygin gas can also be modelled using a scalar field with the Born-Infeld kinetic term [24, 25].

It is interesting that all four of the dark energy models introduced in our paper possess distinct features which allow them to be distinguished from each other at late times. We shall elaborate on these models in the next section.

## 3 Tracker Models of Dark Energy

### 3.1 L-model

Consider first the L-model (2.9) and its natural extension<sup>3</sup>

$$V(\varphi) = V_0 \coth^p \left( \frac{\lambda\varphi}{m_p} \right). \quad (3.1)$$

---

<sup>3</sup>We refer to this model as the ‘L-model’ since  $V(\varphi)$  has a characteristic L shape for large values of  $\lambda$  and  $p$  as shown in figure 1.

For small values of the argument,  $0 < \frac{\lambda\varphi}{m_p} \ll 1$ , one finds

$$V \simeq \frac{V_0}{(\lambda\varphi/m_p)^p} \quad (3.2)$$

which suggests that the early time behaviour of this model is very similar to that of the IPL model for which, at early times [4, 7]

$$w_\varphi = \frac{pw_B - 2}{p + 2}, \quad (3.3)$$

where  $w_B$  is the background equation of state of matter/radiation. The IPL model (3.2) therefore has the appealing property that, for large values of  $p \gg 1$ , its EOS can track the EOS of the dominant matter component in the universe. Unfortunately it is also well known that, for  $\Omega_{0m} \geq 0.2$ , the IPL model (3.2) with  $p > 1$  cannot give rise to  $w_0 < -0.8$  at the present epoch [8]. This may be viewed as a significant shortfall of this model since observations appear to suggest that the current EOS of dark energy should satisfy  $w_0 \leq -0.9$  [13–17]. Of course this problem can be bypassed if one assumes a smaller value  $p < 1$  for the exponent in (3.2). However in this case the initial basin of attraction shrinks considerably, which diminishes the appeal of the IPL model.

In contrast to the IPL model, the L-potential has the following asymptote for  $\frac{\lambda\varphi}{m_p} \gg 1$

$$V(\varphi) \simeq V_0 \quad (3.4)$$

indicating that the L-potential flattens and begins to behave like a cosmological constant at late times. Because of this the present value of the EOS in the L-model can be significantly lower<sup>4</sup> than that in the IPL model (3.2).

The behavior of the L-potential (3.1) is illustrated in Fig. 2. The evolution of the scalar field energy density has been determined by solving the following system of equations relating to a spatially flat Friedman Robertson Walker (FRW) universe

$$H^2 = \frac{8\pi G}{3} (\rho_m + \rho_r + \rho_\varphi) \quad (3.5)$$

$$\ddot{\varphi} + 3H\dot{\varphi} + V'(\varphi) = 0, \quad (3.6)$$

where  $\rho_m$  ( $\rho_r$ ) is the density of matter (radiation), and the density and pressure of the scalar field are

$$\rho_\varphi = \frac{1}{2}\dot{\varphi}^2 + V(\varphi), \quad p_\varphi = \frac{1}{2}\dot{\varphi}^2 - V(\varphi). \quad (3.7)$$

As expected, the early time tracking phase in our model (3.1) – illustrated by figure 3(a), is identical to the tracking phase of the corresponding IPL potential  $V \propto 1/\varphi^p$ .

---

<sup>4</sup>Another means of lowering  $w_0$  is by coupling  $\varphi$  to the Ricci scalar, as shown in [26].

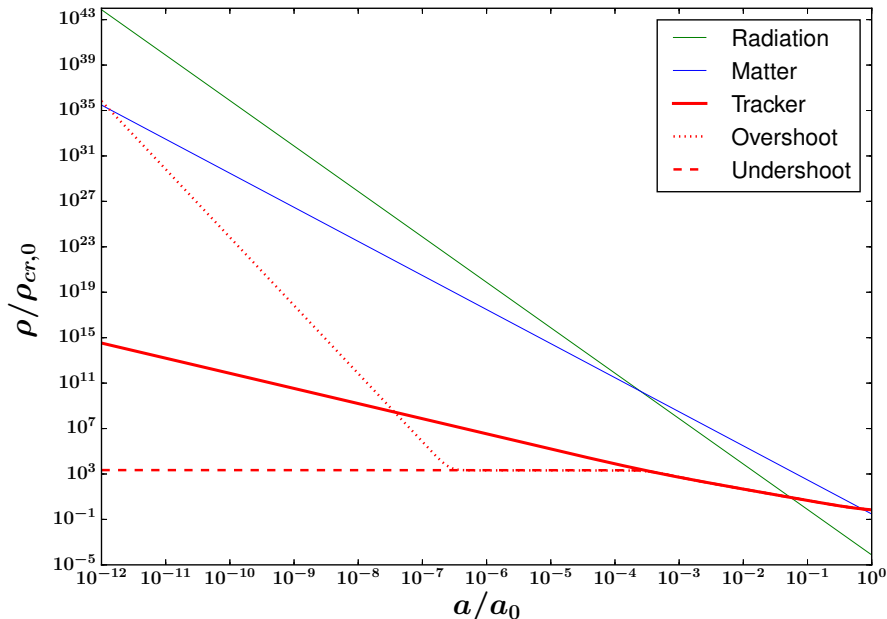


**Figure 2.** This figure illustrates the tracking feature of the L-model  $V = V_0 \coth(\varphi/m_p)$ . The density of the different components is plotted against the scale factor; here  $\rho_{cr,0} \equiv 3m_p^2 H_0^2$  is the current critical density. The solid red curve represents the tracker branch which is similar to that of the corresponding IPL model at early times. Trajectories associated with “overshoot” (dotted red) and “undershoot” (dashed red) initial conditions meet the tracker branch by  $z \sim 10^3$ .

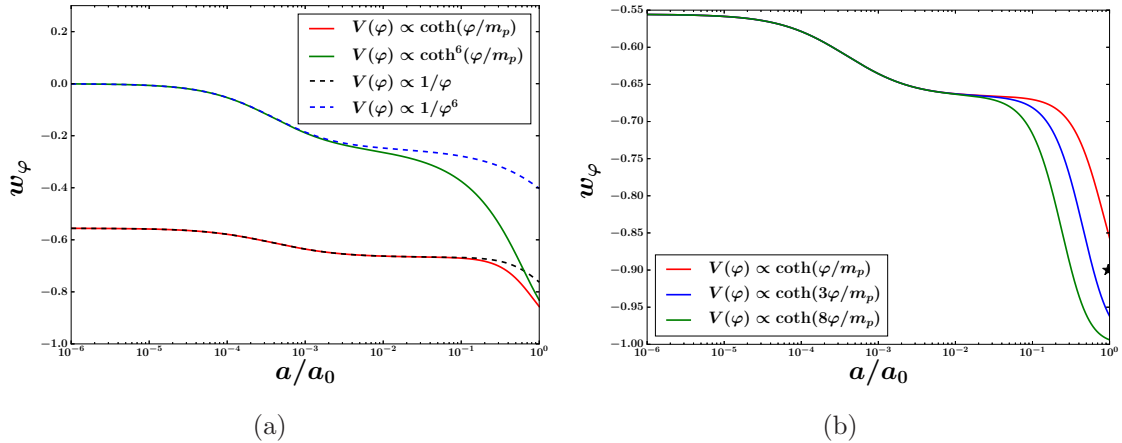
Figure 3(a) shows the evolution of  $w_\varphi(z) = p_\varphi/\rho_\varphi$ , in the L-potential  $V = V_0 \coth^p \varphi/m_p$  and in the IPL potential  $V = V_0 \left(\frac{m_p}{\varphi}\right)^p$ . Note that both potentials have precisely two free parameters:  $V_0$  and  $p$ . Fig. 3(a) draws attention to the interesting fact that, for the L-model with  $V \sim \coth^6 \varphi$ , the current value of  $w_\varphi$  can be as low as  $w_\varphi \sim -0.8$ , which is considerably lower than the corresponding value  $w_\varphi \sim -0.4$  for  $V \sim \varphi^{-6}$ . In other words, for identical values of  $p$ , the late-time value of  $w_\varphi$  in the L-model (3.1) is *significantly lower* than that in the IPL model (3.2). The value of  $w_\varphi$  can be further lowered by increasing the value of  $\lambda$  in (3.1), as shown in figure 3(b). The black star on the right y-axis of figure 3(b) indicates the observational  $2\sigma$  upper bound,  $w_0 \leq -0.9$ , for DE models with a slowly varying EOS<sup>5</sup> [17].

Figure 4 shows the phase-space trajectories of the equation of state  $\{w_\varphi, w'_\varphi\}$  starting from the matter dominated epoch. Here [27, 28]

$$w'_\varphi \equiv \frac{dw_\varphi}{d \ln a} = \frac{\dot{w}_\varphi}{H}. \quad (3.8)$$

<sup>5</sup> The current  $2\sigma$  upper bound on the EOS varies between  $-0.8$  to  $-0.9$ , depending upon the data sets employed and the method of reconstruction [17]. We assume the conservative bound  $w_0 \leq -0.9$  to highlight the fact that the EOS in our models can drop to sufficiently low values at late times.





**Figure 3. (a):** This figure illustrates that the L-model (3.1) possesses early time tracking features similar to that of the inverse power law potential (3.2). However at late times,  $w_\varphi$  in the L-model falls significantly below  $w_\varphi$  in the IPL model. Note that this figure is shown for illustrative purposes and does not reflect current observational constraints on  $w_\varphi$ , which are met by the models in the right panel. **(b):** Increasing the value of  $\lambda$  in (3.1) while keeping  $p$  fixed, makes the current equation of state drop to more negative values. The black star on the right y-axis indicates the (conservative) observational  $2\sigma$  upper bound on  $w_0$  for DE with a slowly varying EOS [17].

Note that all trajectories approach the  $\Lambda$ CDM limit ( $w_\varphi = -1, w'_\varphi = 0$ ) at late times. The present epoch is marked by a circle on each trajectory. Comparing the L-model (3.1) with the IPL potential (3.2) we find that the current EOS in the former is always more negative than that in the latter, *ie*  $w_0^{\text{L}} < w_0^{\text{IPL}}$ , which supports our earlier results in fig. 3(a). Setting  $\lambda = 1$  in (3.1) and increasing the value of  $p$  leads to  $w'_\varphi$  decreasing while  $w_\varphi$  increases. On the other hand, increasing  $\lambda$  (with  $p$  held fixed) leads to the opposite behaviour, namely  $w_\varphi$  decreases whereas  $w'_\varphi$  increases. Note that for moderately large values of  $\lambda$  and  $p$  ( $\lambda, p \sim \text{few}$ ) the L-model (3.1) will have a large initial basin of attraction before converging to  $w_\varphi \sim -1, w'_\varphi \sim 0$  by the present epoch.

### 3.2 Oscillatory tracker model

Next we turn our attention to the oscillatory tracker model (2.10), namely

$$V(\varphi) = V_0 \cosh\left(\frac{\lambda\varphi}{m_p}\right). \quad (3.9)$$

For large values  $\frac{\lambda|\varphi|}{m_p} \gg 1$ , this potential has the asymptotic form

$$V \simeq \frac{V_0}{2} \exp\left(\frac{\lambda\varphi}{m_p}\right). \quad (3.10)$$

The exponential potential has been extensively studied in [4, 6, 11, 29]. In the context of a spatially flat FRW universe it is well known that for  $\lambda^2 > 3(1 + w_B)$  the late time

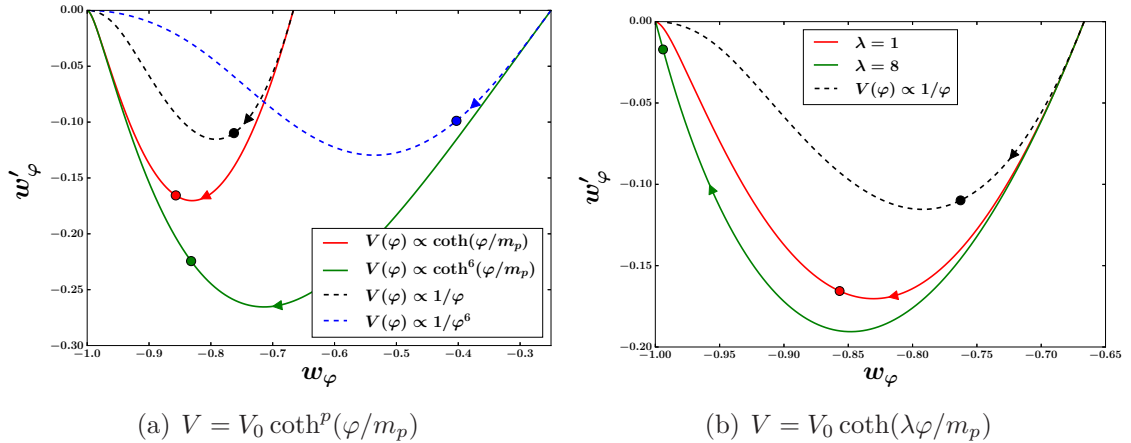


**Figure 4.** Phase space  $\{w_\varphi, w'_\varphi\}$  trajectories for potentials (3.1) and (3.2) starting from the matter dominated epoch. The filled circle on each trajectory represents the present epoch with  $\Omega_{0m} = 0.3$ . Both panels show that in the far future the EOS in all models approaches the  $\Lambda$ CDM value of  $w_\varphi = -1, w'_\varphi = 0$ . The **left panel** demonstrates that with increasing values of  $p$  the current value of  $w_\varphi$  increases while  $w'_\varphi$  decreases. Note that, for identical values of  $p$ , the current values of  $w_\varphi, w'_\varphi$  are much lower in L1 relative to the IPL potential  $V \propto \varphi^{-p}$ . From the **right panel** one finds that an increase in the value of  $\lambda$  leads to a decrease in  $w_\varphi$  and an increase in  $w'_\varphi$ . It is interesting that the different variants of the L-model (3.1) can be easily distinguished from each other and from the IPL potential (3.2). (Note that the left and right panels are not drawn to scale.)

attractor in this model has the same equation of state as the background fluid, namely  $w_\varphi = w_B$ . The associated fractional density of the scalar field is

$$\Omega_\varphi = \frac{3(1 + w_B)}{\lambda^2}, \quad (3.11)$$

with nucleosynthesis constraints imposing the lower bound  $\lambda \gtrsim 5$  [6, 30], while the CMB constraints impose an even stronger lower bound  $\lambda \geq 13$  [31–33].

For small values,  $\frac{\lambda|\varphi|}{m_p} \ll 1$ , the potential (3.9) has the limiting form

$$V(\varphi) \simeq V_0 \left[ 1 + \frac{1}{2} \left( \frac{\lambda\varphi}{m_p} \right)^2 \right]. \quad (3.12)$$

We see that, as in the case of (3.1), the late time asymptote for  $V(\varphi)$  is once again the cosmological constant  $V_0$ . However the presence of  $\varphi^2$  in (3.12) suggests that the late time approach of  $w_\varphi$  to  $-1$  will be oscillatory. This has been illustrated in figures 5, 6 and 7 which show  $w_\varphi(z)$  and  $\{w_\varphi, w'_\varphi\}$  for different values of  $\lambda$ . From figure 5, it is clear that  $w_\varphi = 1/3, 0$  during the radiation and matter domination epochs respectively. However, at late times the scalar field begins to oscillate around the minimum of its potential (3.12). Since these oscillations are of decreasing amplitude,  $w_\varphi$  asymptotically approaches  $w_\varphi = -1$  at late times. Interestingly, for moderate values  $5 \leq \lambda \leq 10$ , the present value of  $w_\varphi$  can lie anywhere between  $-1$  to  $-0.9$ ,

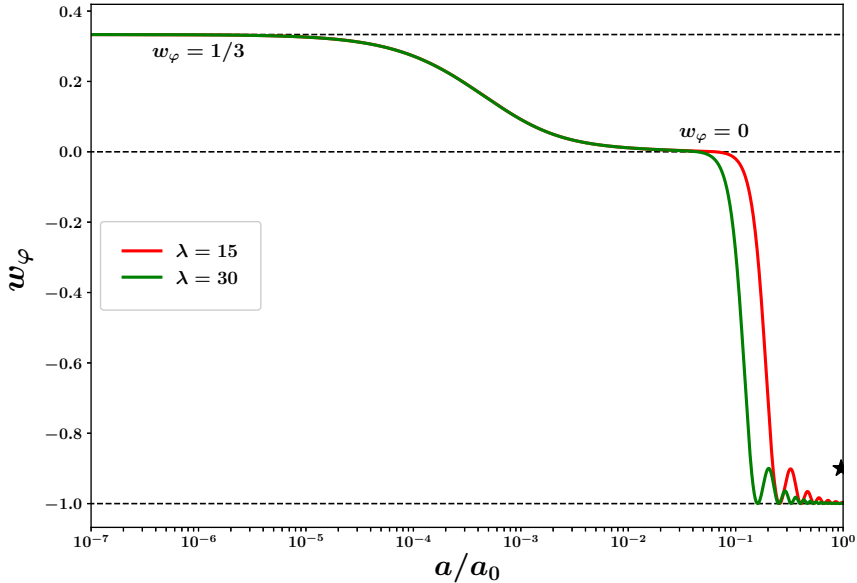


**Figure 5.** This figure illustrates the evolution of the equation of state,  $w_\varphi$ , of the scalar field with the potential  $V(\varphi) = V_0 \cosh\left(\frac{\lambda\varphi}{m_p}\right)$ , for two values of  $\lambda$ . During the radiation and matter dominated epochs, when  $V \sim \exp\left(\frac{\lambda\varphi}{m_p}\right)$ , the scalar field tracks the background density resulting in  $w_\varphi = 1/3, 0$  respectively. At late times, after the commencement of scalar field oscillations, the EOS approaches  $w_\varphi \simeq -1$ , via small oscillations. The black star on the right indicates the (conservative) observational upper bound on  $w_0$  (at  $2\sigma$ ) for DE models with a slowly varying EOS [17]. We show this bound since the dynamical (oscillatory) contribution to  $w_\varphi$  becomes quite small at low  $z$  in our model.

its precise value being determined by the phase of the oscillation. However for larger values  $\lambda > 10$ , the scalar field completes several oscillations prior to the present epoch. Since the mean value of  $\varphi(t)$  in (3.12) falls off as  $\langle\varphi^2(t)\rangle^{1/2} \propto a^{-3/2}(t)$  it follows that in such models  $w_\varphi \simeq -1$  today. This has been illustrated in fig. 5 and especially in fig. 6.

The following expression describes the EOS of dark energy during the oscillatory epoch

$$w_\varphi(t) \simeq -1 + \lambda^2 \left(\frac{\varphi_m(t)}{m_p}\right)^2 \left[1 - \left(\frac{\varphi(t)}{\varphi_m(t)}\right)^2\right], \quad (3.13)$$

where  $\varphi_m(t)$  is the peak oscillation amplitude whose value steadily decreases with time. Eq. (3.13) can be rewritten as

$$w_\varphi(t) \simeq -1 + \frac{\dot{\varphi}^2(t)}{V_0}, \quad (3.14)$$

where the steady decline of  $\dot{\varphi}^2(t)$  with time ensures that  $w_\varphi \rightarrow -1$  at late times.

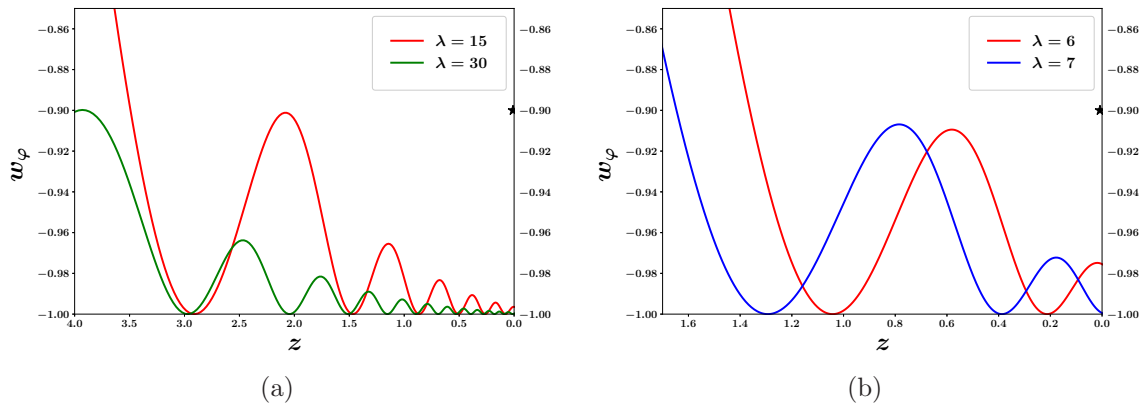


**Figure 6.** **Left panel:** The evolution of  $w_\varphi(z)$  near the present epoch is shown for the potential  $V(\varphi) = V_0 \cosh\left(\frac{\lambda\varphi}{m_p}\right)$  with  $\lambda = 15$  and  $20$ . One finds that although the behaviour of  $w_\varphi(z)$  varies greatly between the two models, all models have certain common features, for instance: (i) the oscillation amplitude decreases with time; (ii) the decreasing oscillation amplitude leads to  $w_\varphi \simeq -1$  at late times. **Right panel:** Models with  $\lambda = 6, 7$  highlight the phase dependence of oscillations for moderate values of  $\lambda$ . In both panels the black star on the right indicates the (conservative) observational upper bound on  $w_0$  (at  $2\sigma$ ) for DE models with a slowly varying EOS [17].

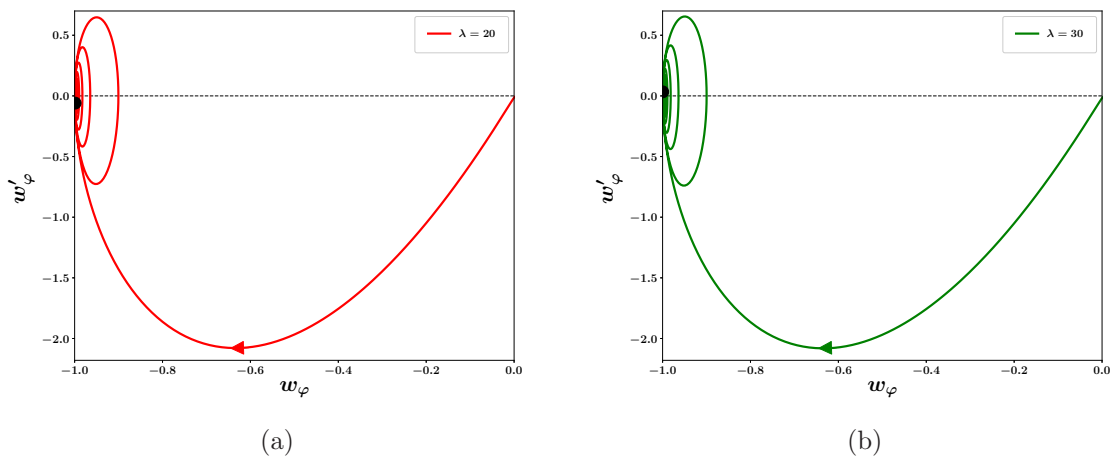


**Figure 7.** The phase-space plot of  $\{w_\varphi, w'_\varphi\}$  for the potential  $V(\varphi) = V_0 \cosh\left(\frac{\lambda\varphi}{m_p}\right)$  with  $\lambda = 20$  (left panel) and  $\lambda = 30$  (right panel) starting from the matter dominated epoch. Arrows depict the flow of time and black circles indicate the present epoch with  $\Omega_{0m} = 0.3$ .

The previous analysis is substantiated by figure 7 which shows the evolution of the phase-space  $\{w_\varphi, w'_\varphi\}$  for  $\lambda = 20, 30$  with filled black circles marking the present epoch ( $\Omega_{0m} = 0.3$ ). The substantial difference in  $w_\varphi(z)$  for  $5 \leq \lambda \leq 30$  and  $0 \leq z \leq 3$  (see fig. 6), may allow such models to be differentiated from one another on the basis

of the high quality data expected from dark energy surveys such as DES, Euclid and SKA.

Due to the presence of the exponential tracker asymptote (3.10), the oscillatory tracker model (3.9) has a very large initial basin of attraction, trajectories from which get funneled into the late time attractor  $w_\varphi \simeq -1$ . Our results, summarized in figure 8, demonstrate that initial density values covering a range of more than 40 orders of magnitude at  $z = 10^{12}$ , converge onto the attractor scaling solution represented by the solid red curve. This range substantially increases if we set our initial conditions at earlier times. For instance, upon setting  $\{\varphi_i, \dot{\varphi}_i\}$  at the GUT scale of  $10^{14}$  GeV ( $z \sim 10^{26}$ ), the range of initial density values that converges to  $\Omega_{0,\text{DE}} \simeq 0.7$  spans an impressive 100 orders of magnitude! The oscillatory tracker potential therefore exhibits a very large degree of freedom in the choice of initial conditions. In particular it permits the possibility of equipartition, according to which the density of dark energy and radiation may have been comparable at very early times just after reheating. In our view this is a very compelling property of this DE model.<sup>6</sup>

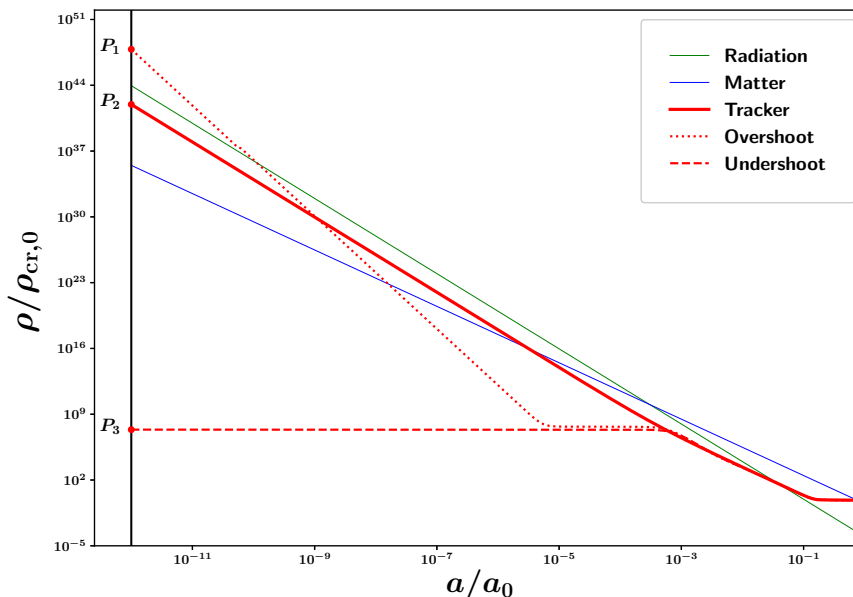


**Figure 8.** The evolution of the scalar-field density (red; in units of  $\rho_{\text{cr},0} \equiv 3m_p^2 H_0^2$ ) is shown together with the density in radiation (green) and matter (blue). The scalar field commences its descent from the exponential tracker asymptote of the potential  $V(\varphi) = V_0 \cosh\left(\frac{\lambda\varphi}{m_p}\right)$  with  $\lambda = 15$ . One finds that a very large range in initial scalar-field density values, covering over 40 orders of magnitude at  $z \simeq 10^{12}$  ( $P_1$  to  $P_3$ ) leads to  $\Omega_{0,\text{DE}} \simeq 0.7$  today.  $P_2$  marks the initial density corresponding to the attractor solution (solid red) to which all trajectories within the  $P_1$ – $P_3$  range converge by  $z \sim 100$ .

<sup>6</sup> See [34, 35] for a dynamical analysis of models based on similar potentials.

In passing it may be appropriate to point out that the CPL ansatz [36, 37]

$$w(a) = w_0 + w_1(1 - a) = w_0 + w_1 \frac{z}{1 + z}, \quad (3.15)$$

which is frequently used to reconstruct the properties of DE from observations, may be unable to accommodate the oscillatory behaviour of  $w_\varphi$  which characterizes this model. Non-parametric reconstruction is likely to work better for this class of potentials [2, 38–40].

Note that the companion potential to (3.9),

$$V(\varphi) = V_0 \sinh^2 \frac{\tilde{\lambda}\varphi}{m_p} \quad (3.16)$$

describes a tracker model of dark matter for  $V_0 \tilde{\lambda}^2 / m_p^2 \gg H_0^2$  [20]. It is therefore interesting that, when taken together, the pair of  $\alpha$ -attractor potentials (3.9) and (3.16) with  $\tilde{\lambda} \gg \lambda$ , can describe tracker models of both dark matter *and* dark energy !

### 3.3 The Recliner model

The recliner potential<sup>7</sup>

$$V(\varphi) = V_0 \left[ 1 + \exp\left(-\frac{\lambda\varphi}{m_p}\right) \right], \quad (3.17)$$

possesses the asymptotic form  $V \simeq V_0 \exp(-\frac{\lambda\varphi}{m_p})$  for  $\lambda|\varphi| \gg m_p$  ( $\varphi < 0$ ). This endows it with a large initial basin of attraction, due to which scalar field trajectories rolling down (3.17) approach a common evolutionary path from a wide range of initial conditions. In the large  $\varphi$  limit,  $\lambda\varphi \gg m_p$ ,  $V(\varphi)$  monotonically declines to  $V(\varphi) \simeq V_0$ . Therefore one expects the value of  $w_\varphi$  to approach  $w_\varphi \rightarrow -1$  at late times, without any intermediate oscillations. This behaviour is substantiated by figure 9. The fact that the current value of  $w_\varphi$  can fall below  $-0.9$  makes this model quite appealing since it can describe cosmic acceleration without the fine tuning of initial conditions. The evolution of  $w_\varphi(z)$  near the present epoch is shown in figure 10. One finds that different values of  $\lambda$  in (3.17) can clearly be distinguished on the basis of low redshift measurements of  $w_\varphi(z)$ . Consequently upcoming dark energy survey’s (DES, Euclid, SKA, etc.) may provide a unique opportunity to set bounds (or even determine) the value of  $\lambda$  in (3.17). Phase-space trajectories  $\{w_\varphi, w'_\varphi\}$  for the Recliner potential (3.17) are illustrated in figure 11. Note that larger values of  $\lambda$  in (3.17) result in smaller values of  $w_\varphi$  and larger values of  $w'_\varphi$  at late times.

It is interesting that the Oscillating tracker potential (3.9) and the Recliner potential(3.17) have two free parameters each,  $V_0$  and  $\lambda$ , precisely the same number as in the IPL model  $V = V_0\varphi^{-p}$  and the tracker  $V = V_0 \exp\left(-\frac{\lambda\varphi}{m_p}\right)$ .

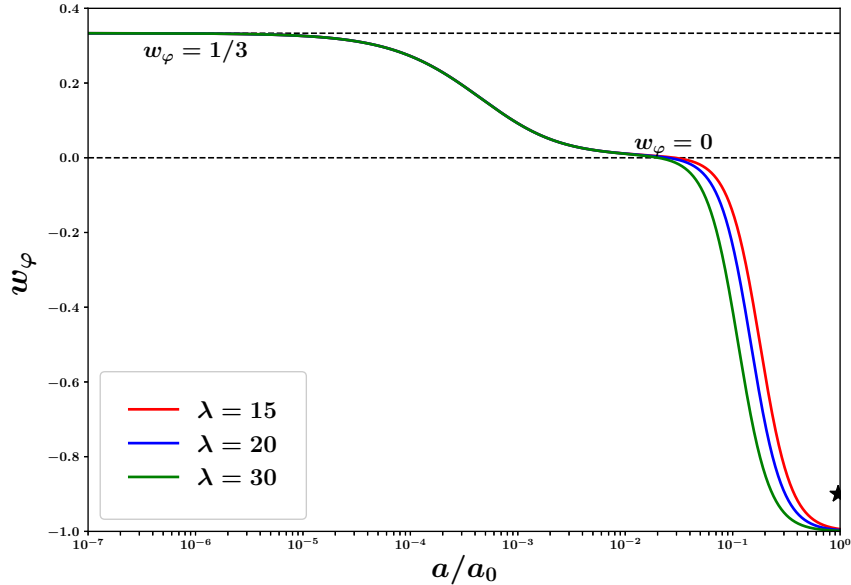


**Figure 9.** This figure illustrates the evolution of  $w_\varphi$  for the potential  $V(\varphi) = V_0 \left[ 1 + \exp\left(-\frac{\lambda\varphi}{m_p}\right) \right]$ , for different values of  $\lambda$ . One finds that during the radiation and matter dominated epochs, when  $V \simeq V_0 \exp\left(-\frac{\lambda\varphi}{m_p}\right)$ , the scalar field tracks the cosmological background density with  $w_\varphi = 1/3$ ,  $0$  respectively. However at late times the value of  $w_\varphi$  sharply drops and approaches  $w_\varphi = -1$  asymptotically. Larger values of  $\lambda$  result in more negative values of  $w_\varphi$  at late times. The black star on the right indicates the (conservative) observational upper bound on  $w_0$  (at  $2\sigma$ ) for DE models with a slowly varying EOS [17].

### 3.4 Transient dark energy from the Margarita potential

The Margarita potential describes a model of transient dark energy

$$V(\varphi) = V_0 \tanh^2\left(\frac{\lambda_1\varphi}{m_p}\right) \cosh\left(\frac{\lambda_2\varphi}{m_p}\right), \quad \lambda_1 \gg \lambda_2. \quad (3.18)$$

This potential has tracker-like wings and a flat intermediate region (see figure 12). It exhibits three asymptotic branches:

$$\text{Tracker wing: } V(\varphi) \simeq \frac{V_0}{2} \exp(\lambda_2|\varphi|/m_p), \quad \frac{|\varphi|}{m_p} \gg \frac{1}{\lambda_2}, \quad (3.19)$$

$$\text{Flat wing: } V(\varphi) \simeq V_0 + \frac{1}{2}m_2^2\varphi^2, \quad \frac{1}{\lambda_1} \ll \frac{|\varphi|}{m_p} \ll \frac{1}{\lambda_2}, \quad (3.20)$$

$$\text{Oscillatory region: } V(\varphi) \simeq \frac{1}{2}m_1^2\varphi^2, \quad \frac{|\varphi|}{m_p} \ll \frac{1}{\lambda_1}, \quad (3.21)$$

<sup>7</sup>The Recliner potential (3.17) presents a limiting case of the family of potentials studied in [11], also see [33].

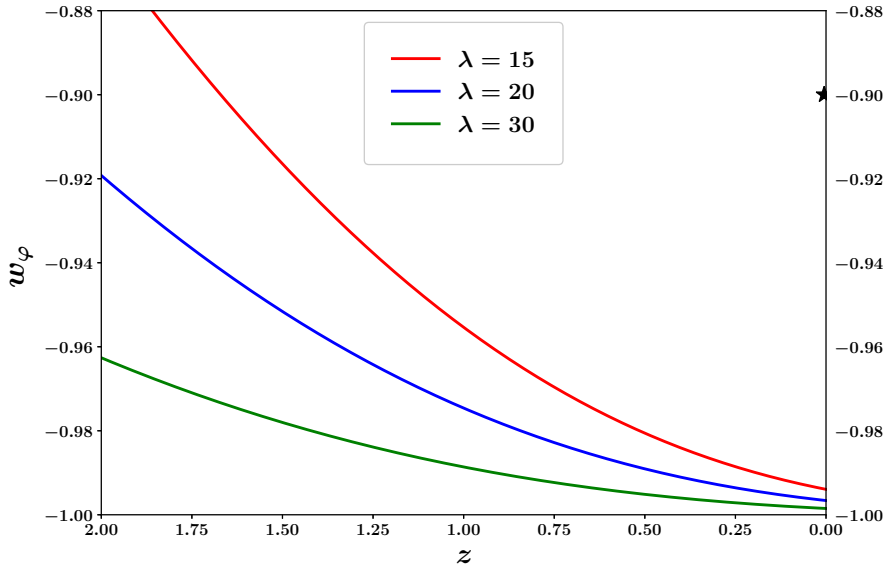


**Figure 10.** The evolution of  $w_\varphi(z)$  for the potential (3.17) is shown for  $\lambda = 15, 20, 30$ . One notes that larger values of  $\lambda$  lead to a more negative equation of state. The black star on the right indicates the observational (conservative) upper bound on  $w_0$  at  $2\sigma$  for DE models with a slowly varying EOS [17].

where  $m_1^2 = \frac{2V_0\lambda_1^2}{m_p^2}$  and  $m_2^2 = \frac{V_0\lambda_2^2}{m_p^2}$  with  $m_1 \gg m_2$ .

As illustrated by the red curve in figure 13, the acceleration of the universe in this model is a transient phenomenon. It ends once the scalar field rolls to the minimum of  $V(\varphi)$ . From that point on the scalar field begins to oscillate and behave like dark matter. Consequently the universe reverts to matter dominated expansion after the current accelerating epoch is over, with an extra contribution to dark matter coming from the coherently oscillating scalar field.

As suggested by (3.19) – (3.21), the motion of the scalar field proceeds along three distinct stages each of which is reflected in the cosmic expansion history.

(i) Initially  $\varphi(t)$  rolls down the exponential potential (3.19). During this phase the scalar field density scales like the background fluid (radiation/matter) driving the expansion of the universe. (ii) After the tracking phase is over, the scalar field oscillates around the *flat wing* of the potential shown in figure 12. During this phase the universe begins to accelerate, as demonstrated in figure 14. (iii) Finally, at late times, the scalar field gets trapped within the sharp *oscillatory region* of the potential (3.21); see figure 12. Oscillations of the scalar field during this stage make it behave like pressureless matter with  $\langle w_\varphi \rangle = 0$ ; see the red line in figures 13 and 16.

We therefore find that cosmic acceleration is sandwiched between two matter dominated epochs. The duration of the accelerating phase depends upon the gap between  $\lambda_1$  and  $\lambda_2$ . Nucleosynthesis constraints limit  $\lambda_2 \geq 5$  whereas the only constraint on  $\lambda_1$  comes from the inequality  $\lambda_1 \gg \lambda_2$ .



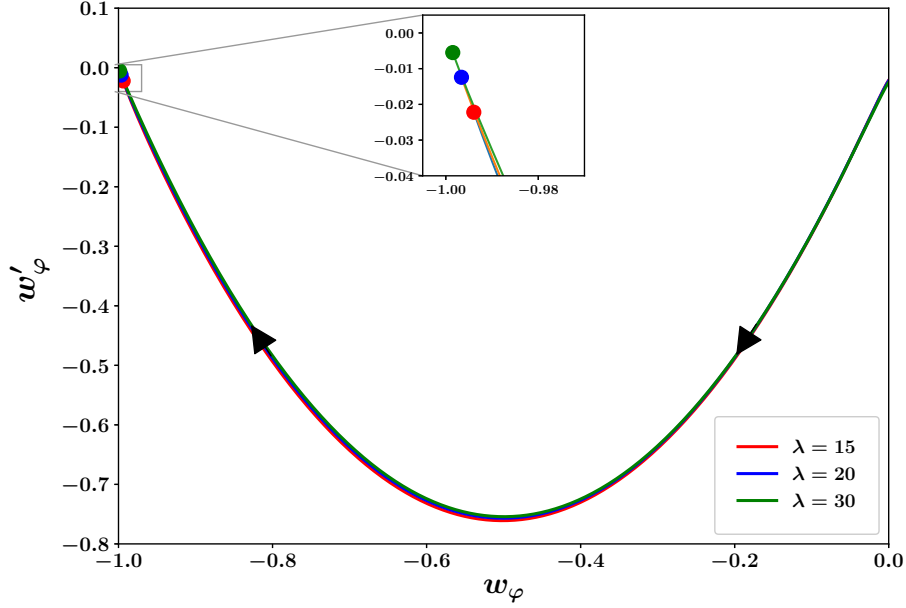


**Figure 11.** Phase-space  $\{w_\varphi, w'_\varphi\}$  trajectories for the potential  $V(\varphi) = V_0 \left[ 1 + \exp\left(-\frac{\lambda\varphi}{m_p}\right) \right]$  are shown for different values of  $\lambda$  starting from the matter dominated epoch. The large colored circles correspond to the present epoch ( $z = 0$ ) in each of the three models. Arrows depict the flow of time. One finds that larger values of  $\lambda$  result in smaller values of  $w_\varphi$  and larger values of  $w'_\varphi$  at late times.

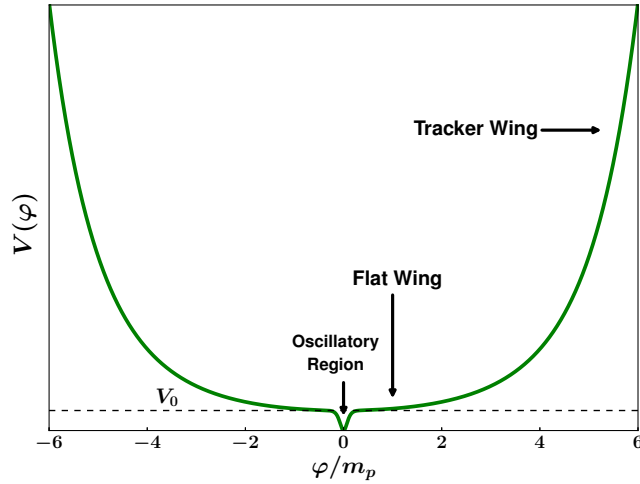


**Figure 12.** This figure schematically illustrates the transient DE potential (3.18) with  $\lambda_1 = 10$  and  $\lambda_2 = 1$ . The main features of this potential are: exponential tracker wings for  $\frac{|\varphi|}{m_p} \gg \frac{1}{\lambda_2}$ , flat wings for  $\frac{1}{\lambda_1} \ll \frac{|\varphi|}{m_p} \ll \frac{1}{\lambda_2}$ , and an oscillatory region ( $\frac{|\varphi|}{m_p} \ll \frac{1}{\lambda_1}$ ) where  $V \propto \varphi^2$ .

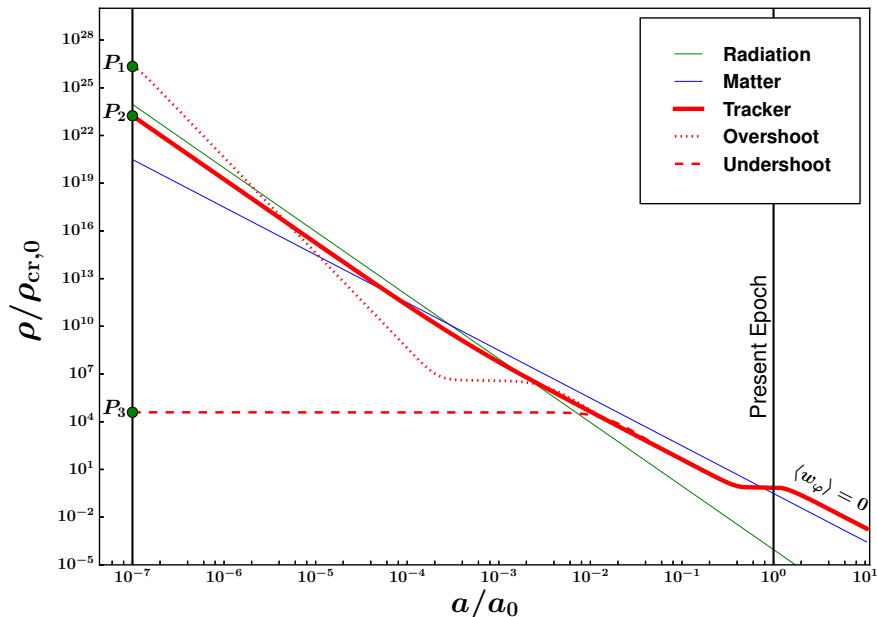


**Figure 13.** The evolution of the scalar-field density (red), in units of  $\rho_{\text{cr},0} = 3m_p^2 H_0^2$ , is shown from  $z \simeq 10^7$  until  $z = 0$ . The scalar field commences its descent from the exponential tracker asymptote of the potential (3.18) with  $\lambda_1 = 500$  and  $\lambda_2 = 5$ . A large range in initial (scalar-field) density values, covering more than 20 orders of magnitude from  $P_1$  to  $P_3$ , leads to  $\Omega_{0,\text{DE}} \simeq 0.7$  today.  $P_2$  marks the initial density corresponding to the attractor solution (solid red) to which all trajectories commencing in the  $P_1$ – $P_3$  range converge. Note that cosmic acceleration is a transient phenomenon since the universe reverts to matter domination in the future once the scalar field begins to oscillate with  $\langle w_\varphi \rangle = 0$ .

At this point we would like to draw attention to a key feature of the Margarita potential which distinguishes this model of transient acceleration from others of its kind. Note that the asymptotic form of the potential within the flat wing, described by (3.20), bears close resemblance to the potential near  $\varphi \simeq 0$  for the oscillatory tracker model, namely (3.12). Therefore, as in that model, one might expect  $w_\varphi$  to approach  $-1$  at late times via small oscillations. This would indeed be the case were it not for the presence of the sharp *oscillatory region* near  $\varphi \simeq 0$  in fig. 12. This region modifies the behaviour of  $\varphi$  significantly. As  $\varphi$  traverses  $\varphi \simeq 0$ , its EOS abruptly changes from negative to positive values. This leads to a spike in the value of  $w_\varphi$  and in the deceleration parameter  $q$ . An accelerating universe punctuated by periods of sudden deceleration therefore becomes a key feature of the Margarita model of DE, as shown in figures 14 & 15.

It is well known that, unlike  $\Lambda\text{CDM}$ , a transiently accelerating universe does not possess a future event horizon. Moreover the presence of even a tiny curvature term,  $k/a^2$ , can cause such a universe to stop expanding and begin to contract, giving rise to a very different cosmological future from  $\Lambda\text{CDM}$ . Note that while models of transient

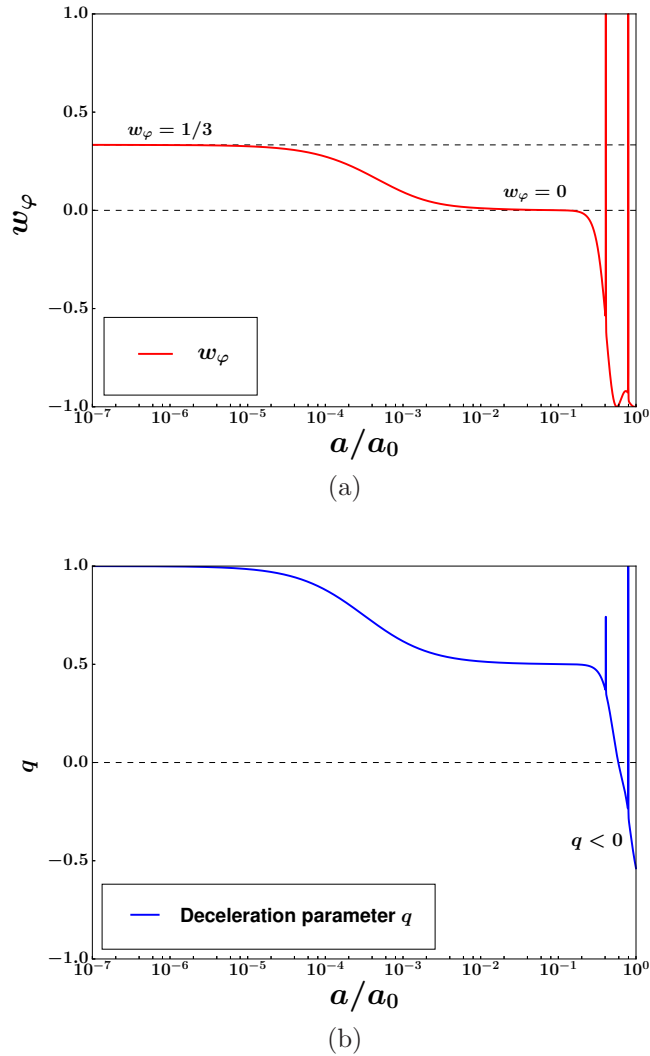


**Figure 14.** The evolution of  $w_\varphi$  (upper panel) and the deceleration parameter  $q = -\frac{\ddot{a}}{aH^2}$  (lower panel) is shown for the transient DE model (3.18) with  $\lambda_1 = 500$  and  $\lambda_2 = 5$ . One finds that during the radiation and matter dominated epochs the scalar field tracks the cosmological background density with  $w_\varphi = 1/3$ , 0 respectively. However at late times the scalar field gets trapped within the flat wing of the Margarita potential shown in fig. 12. When this happens  $\varphi(t)$  begins to oscillate within the flat wing and  $w_\varphi$  drops to negative values, signifying cosmic acceleration. It is interesting that the oscillatory epoch is punctuated by sharp spikes in  $w_\varphi$  and  $q$ . Spikes occur whenever  $\varphi(t)$  ventures inside the sharp potential well at  $\varphi(t) \simeq 0$ , see fig. 12. When this happens  $w_\varphi$  and  $q$  abruptly increase and, for a very brief period of time, acceleration  $q < 0$  gives way to deceleration  $q > 0$ . A magnified view of this region is shown in the next figure. Finally, in the distant future,  $\varphi$  gets trapped within the *oscillatory region* near  $\varphi \simeq 0$  shown in fig. 12. At this point rapid oscillations of  $\varphi(t)$  ensure that the effective equation of state is pressureless,  $\langle w_\varphi \rangle = 0$ , and the universe expands as if matter dominated; see fig. 16.

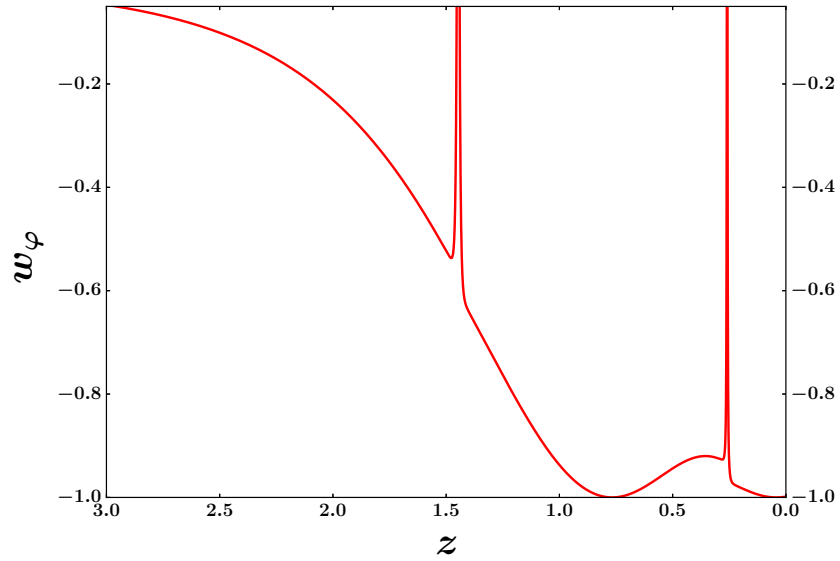


**Figure 15.** The presence of spikes in the EOS of dark energy is highlighted by this figure. Spikes arise whenever  $\varphi(t)$  traverses the region near the origin  $\varphi \simeq 0$  where  $V(\varphi)$  has a sharp feature; see fig. 12.

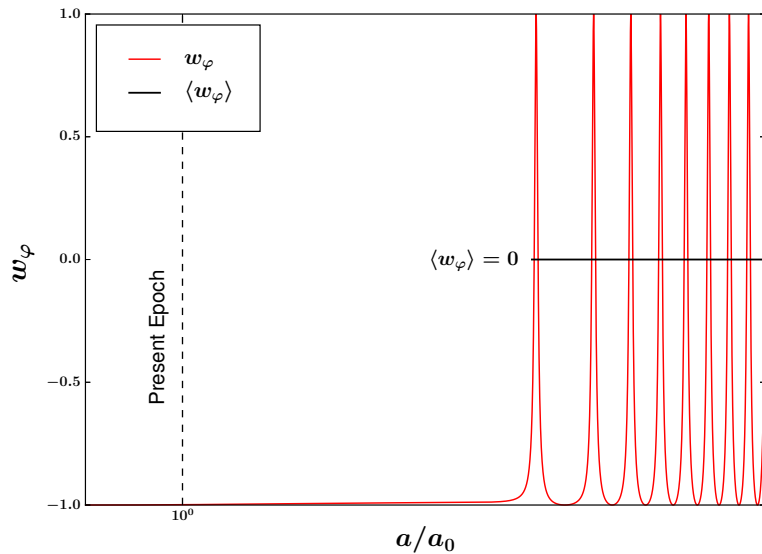


**Figure 16.** The future evolution of  $w_\varphi$  is shown for the transient DE model (3.18). Note that the scalar field behaves almost like a cosmological constant ( $w_\varphi \simeq -1$ ) close to the present epoch. At late times rapid oscillations of  $\varphi(t)$  (within the *oscillatory region* of figure 12) result in the scalar field behaving like pressureless (dark) matter with  $\langle w_\varphi \rangle = 0$ . Thus the present accelerating epoch is sandwiched between two matter dominated epochs.

DE have been discussed earlier, see for instance [41–43], to the best of our knowledge none of these early models had a tracker-like commencement.

Finally the reader may be interesting in a companion potential to (3.18) which provides another example of transient dark energy with tracker-like behaviour at early times

$$V(\varphi) = V_0 \left( 1 - e^{-\left(\frac{\lambda_1 \varphi}{m_p}\right)^2} \right) \cosh \left( \frac{\lambda_2 \varphi}{m_p} \right), \quad \lambda_1 \gg \lambda_2. \quad (3.22)$$

## 4 Discussion

In this paper we discuss four new models of dark energy based on the  $\alpha$ -attractor family. In all of these models the present value of the equation of state can fall below  $-0.9$ , in agreement with recent observations. This does not come at the expense of finely tuned initial conditions, since all of the four models display tracker-like behaviour at early times. The initial attractor basin is largest for the Oscillatory tracker model (2.10), the Recliner potential (2.11) and the Margarita potential (2.12), in all of which  $V \propto e^{\lambda\varphi}$  at early times. The fourth model, which is described by the L-potential (2.9), has exactly the same basin of attraction as the inverse power law potential  $V \propto \varphi^{-p}$ . It is interesting that all of these models display distinct late time features which allow them to be easily distinguished from one another. For instance, in the Oscillatory tracker model (2.10) the late-time attractor  $w_\varphi \simeq -1$  is reached through a series of oscillations of decreasing amplitude. By contrast, oscillations in  $w_\varphi$  are absent in the Recliner potential (2.11), in which the late-time approach to  $w_\varphi \simeq -1$  occurs via a steady decline in the value of  $w_\varphi$ .

Our fourth model, represented by the Margarita potential (2.12), describes a *transient* model of dark energy. In this model the accelerating phase is sandwiched between two matter dominated epochs. However unlike other transiently accelerating models discussed in the literature, the Margarita potential provides us with an example of an  $\alpha$ -attractor based model with a tracker-like asymptote at early times. This ensures that transient acceleration can arise from a fairly large family of initial conditions.

Finally we would like to mention that the potentials suggested in this paper do not claim to address the ‘why now’ question which is sometimes raised in the context of dark energy. The potentials in our paper contain two free parameters  $V_0$  and  $\lambda$ . The value of  $\lambda$  is chosen in keeping with the requirement that the EOS can drop to the low values demanded by observations [17]. The value of the other free parameter  $V_0$  is adjusted to ensure  $\Omega_m \simeq 1/3$ ,  $\Omega_{\text{DE}} \simeq 2/3$  at the present epoch. Its important to note that for a given value of  $V_0$  there is an entire range of initial conditions  $\{\varphi_i, \dot{\varphi}_i\}$  which funnel dark energy to its present value. This ensures that there is little fine tuning of initial conditions in the models discussed in this paper.

## Acknowledgments

The authors acknowledge useful discussions with Yu. Shtanov and A. Viznyuk. S.B. and S.S.M. thank the Council of Scientific and Industrial Research (CSIR), India, for financial support as senior research fellows.

## A Can $\Lambda$ CDM cosmology emerge from a single oscillatory potential ?

Consider any potential such as  $V = V_0 \cosh \lambda\varphi/m_p$  in (3.9) which has an early time tracker phase and the late time asymptotic form

$$V(\varphi) \simeq V_0 \left[ 1 + \frac{1}{2} \left( \frac{\lambda\varphi}{m_p} \right)^2 \right], \quad |\lambda\varphi| \ll m_p. \quad (\text{A.1})$$

Recasting (A.1) as

$$V(\varphi) \simeq V_0 + \frac{1}{2} m^2 \varphi^2, \quad (\text{A.2})$$

where  $m^2 = \frac{V_0 \lambda^2}{m_p^2}$ , one might be led into thinking that: (i) since  $V_0$  behaves like the cosmological constant, and (ii) the  $m^2 \varphi^2$  term leads to oscillations in  $\varphi$  during which  $\langle w_\varphi \rangle \simeq 0$ , therefore a potential having the general asymptotic form (A.2) might be able to play the dual role of describing both dark matter and dark energy. However this is not the case for the simple reason that although oscillations commence when  $m \gtrsim H$ , which might lead one to believe that  $\frac{1}{2} m^2 \varphi^2 \gg V_0$ , the asymptotic forms (A.1) and (A.2) are only valid in the limit  $|\lambda\varphi| \ll m_p$  which implies  $\frac{1}{2} m^2 \varphi^2 \ll V_0$ . In other words, the cosmological constant  $V_0$  is always larger than the oscillatory  $m^2 \varphi^2$  term soon after the onset of oscillations, leaving little room for a prolonged dark matter dominated epoch as demanded by observations.

Note, however, that a viable model of  $\Lambda$ CDM based on a single scalar field can be constructed within the framework of a non-canonical Lagrangian, as shown in [44].

## References

- [1] V. Sahni and A.A. Starobinsky, *Int. J. Mod. Phys.* **D9** 373 (2000).
- [2] V. Sahni and A.A. Starobinsky, *Int. J. Mod. Phys.* **D15** 2105 (2006).
- [3] P. J. E. Peebles and B. Ratra, *Rev. Mod. Phys.* **75** 559 (2003); T. Padmanabhan, *Phys. Rep.* **380** 235 (2003); V. Sahni, [astro-ph/0202076], [astro-ph/0502032]; V. Sahni, *Dark matter and dark energy*, *Lect. Notes Phys.* 653, 141-180 (2004) [astro-ph/0403324]. E. J. Copeland, M. Sami and S. Tsujikawa, *Int. J. Mod. Phys.* **D15** 1753 (2006); R. Bousso, *Gen. Relativ. Gravit.* **40**, 607 (2008); L. Amendola and S. Tsujikawa, *Dark Energy*, Cambridge University Press, 2010.
- [4] B. Ratra and P.J.E. Peebles, *Phys. Rev. D* **37**, 3406 (1988).
- [5] C. Wetterich, *Nuclear Physics B* **302**, 668 (1988).
- [6] P.G. Ferreira and M. Joyce, *Phys. Rev. Lett.* **79**, 4740 (1997); P.G. Ferreira, P.G. and M. Joyce, *Phys. Rev. D* **58**, 023503 (1998).
- [7] I. Zlatev L. Wang and P.J. Steinhardt, *Phys. Rev. Lett.* **82**, 896 (1999).
- [8] P.J. Steinhardt, L. Wang and I. Zlatev, *Phys. Rev. D* **59**, 123504 (1999).
- [9] V. Sahni and L. Wang, *Phys. Rev. D* **62**, 103517 (2000).

- [10] P. Brax and J. Martin, Phys. Rev. D **61**, 103502 (2000); Phys. Lett. B **468**, 40 (1999).
- [11] T. Barreiro, E.J. Copeland and N.J. Nunes, Phys. Rev. D **61**, 127301 (2000).
- [12] A. Albrecht and C. Skordis, Phys. Rev. Lett. **84**, 2076 (2000).
- [13] Y. Wang et al., SDSS Collaboration, MNRAS **469**, 3762 (2017) [arXiv:1607.03154].
- [14] S. Alam et al., BOSS Collaboration, MNRAS **470**, 2617 (2017) [arXiv:1607.03155].
- [15] P.A.R. Ade et al., Planck Collaboration, Astron. Astrophys. **594**, A14 (2016), Dark energy and modified gravity, [arXiv:1502.01590].
- [16] A. I. Lonappan, Ruchika, A. A Sen, arXiv:1705.07336.
- [17] D. Huterer and D.L. Shafer, Rep. Prog. Phys. **81**, 016901 (2018) [arXiv:1709.01091].
- [18] R. Kallosh and A. Linde, JCAP07 (2013) 002 [arXiv:1306.5220].
- [19] R. Kallosh, A. Linde and D. Roest, JHEP11, 198 (2013) [arXiv:1311.0472].
- [20] S. Mishra, V. Sahni and Yu. Shtanov, JCAP 06(2017)045 [arXiv:1703.03295]
- [21] E. V. Linder, Phys. Rev. D **91**, no. 12, 123012 (2015) [arXiv:1505.00815].
- [22] A. Kamenshchik, U. Moschella and V. Pasquier, 2001, Phys. Lett. B **511**, 265 [gr-qc/0103004].
- [23] V. Gorini, A. Kamenshchik, U. Moschella, V. Pasquier and A. Starobinsky, 2005, Phys. Rev. D **72**, 103518 [astro-ph/0504576].
- [24] N. Bilic, G.B. Tupper and R. Viollier, 2002, Phys. Lett. B **535**, 17 [astro-ph/0111325].
- [25] A. Frolov, L. Kofman and A. Starobinsky, 2002, Phys. Lett. B **545**, 8 [hep-th/0204187].
- [26] S. Matarrese, C. Baccigalupi and F. Perrotta, Phys. Rev. D **70**, 061301 (2004).
- [27] R.R. Caldwell and E.V. Linder, Phys. Rev. Lett. **95**, 141301 (2005).
- [28] E.V. Linder, Astropart. Phys. **91**, 11 (2017) [arXiv:1701.01445].
- [29] V. Sahni, H. Feldman and A. Stebbins, Astrophys.J. **385**, 1, (1992).
- [30] E.J. Copeland, A.R. Liddle and D. Wands, Phys. Rev. D **57**, 4686 (1998).
- [31] E. Calabrese, D. Huterer, E. V. Linder, A. Melchiorri and L. Pagano, Phys. Rev. D **83**, 123504 (2011) [arXiv:1103.4132 [astro-ph.CO]].
- [32] A. Hojjati, E. V. Linder and J. Samsing, Phys. Rev. Lett. **111**, 041301 (2013) [arXiv:1304.3724 [astro-ph.CO]].
- [33] H. Chang, R. J. Scherrer, [arXiv:1608.03291].
- [34] N. Roy and N. Banerjee, Gen. Rel. Grav. **46**, 1651 (2014) [arXiv:1312.2670 [gr-qc]].
- [35] A. Paliathanasis, M. Tsamparlis, S. Basilakos and J. D. Barrow, Phys. Rev. D **91**, no. 12, 123535 (2015) [arXiv:1503.05750 [gr-qc]].
- [36] M. Chevallier and D. Polarski, Int. J. Mod. Phys. D **10**, 213 (2001) [gr-qc/0009008].
- [37] E. V. Linder, Phys. Rev. Lett. **90**, 091301 (2003) [astro-ph/0208512].

- [38] A. Shafieloo, U. Alam, V. Sahni, and A.A. Starobinsky, *Mon. Not. R. Astron. Soc.* **366**, 1081 (2006); J. Dick, L. Knox, and M. Chu, *J. Cosmol. Astropart. Phys.* 07 (2006) 001; A. Shafieloo, *Mon. Not. R. Astron. Soc.* **380**, 1573 (2007); D. Huterer and G. Starkman, *Phys. Rev. Lett.* **90**, 031301 (2003); R. G. Crittenden, L. Pogosian, and G. B. Zhao, *J. Cosmol. Astropart. Phys.* 12 (2009) 025; C. Clarkson and C. Zunckel, *Phys. Rev. Lett.* **104**, 211301 (2010); R. G. Crittenden, G. B. Zhao, L. Pogosian, L. Samushia, and X. Zhang, *J. Cosmol. Astropart. Phys.* 02 (2012) 048; T. Holsclaw, U. Alam, B. Sanso, H. Lee, K. Heitmann, S. Habib, and D. Higdon, *Phys. Rev. Lett.* **105**, 241302 (2010); A. Shafieloo, A. G. Kim, and E.V. Linder, *Phys. Rev. D* **85**, 123530 (2012); M. Seikel, C. Clarkson, and M. Smith, *J. Cosmol. Astropart. Phys.* 06 (2012) 036.
- [39] G-B. Zhao, R. G. Crittenden, L. Pogosian and X. Zhang, *Phys. Rev. Lett.* **109**, 171301 (2012).
- [40] G-B Zhao, et. al., *Nature Astronomy* **1**, 627 (2017).
- [41] J. Frieman, C.T. Hill, A. Stebbins and I. Waga, *Phys. Rev. Lett.* **75**, 2077 (1995); K. Choi, *Phys. Rev. D* **62** 043509 (2000) [hep-ph/9902292]; J.D. Barrow, R. Bean, and J. Magueijo, *MNRAS* **316**, L41 (2000); S.C. Ng and D.L. Wiltshire, *Phys. Rev. D* **64** 123519 (2001) [astro-ph/0107142]; R. Kallosh, A. Linde, S. Prokushkin and M. Shmakova, *Phys. Rev. D* **66** 123503 (2002) [arXiv:hep-th/0208156]; R. Kallosh and A. Linde, *JCAP* **02** 02 (2003) [astro-ph/0301087]; U. Alam, V. Sahni and A.A. Starobinsky, *JCAP* **0304**, 002 (2003) [astro-ph/0302302].
- [42] V. Sahni and Yu.V. Shtanov *JCAP* 0311,014, (2003) [astro-ph/0202346](#).
- [43] A. Shafieloo, D.K. Hazra, V. Sahni and A. A. Starobinsky, *Metastable Dark Energy with Radioactive-like Decay*, arXiv:1610.05192.
- [44] V. Sahni and A. A. Sen, *Eur.Phys.J.* **C77**, 225 (2017) [arXiv:1510.09010]